ENERGY ABSORPTION DURING FLEXURAL FAILURE OF LAYERED METAL FOAM / CERAMIC COMPOSITES

A.E.Markaki and T.W.Clyne

Department of Materials Science, Cambridge University, Pembroke Street, Cambridge CB2 3QZ, UK.

SUMMARY: Laminates consisting of alternate layers of Al_2O_3 and foamed Al alloy have been prepared using a hot-pressing technique. The foamed metal constituent was either Al-7Si or Al-12Si-0.6Mg. Mechanical tests have been performed using several specimen configurations. These include laminate flexure and constrained tensile fracture of single metal foam layers. Comparisons are presented between measured fracture energies during bending and predictions based on the deformation behaviour of bridging ligaments. The deformation characteristics of multi-layer laminates and single constrained foam layers are compared with those observed for dense metal layers of the same composition. It was found that the fracture energy of the laminates increased with increasing proportion of the foam layers, as predicted theoretically. Part of the energy is absorbed by plastic deformation of the metallic constituent, as with fully dense laminates, but there is some evidence that another process, such as frictional sliding at the interface, may also have made a significant contribution.

KEYWORDS : Metallic Composites, Foams, Porosity, Layered Structures

INTRODUCTION

It is now well documented that layered metal / ceramic systems have the potential to exhibit attractive combinations of low density with high strength, stiffness and toughness[1-7]. One approach to minimisation of weight in such systems is to replace the solid metal layers with foamed metal. The toughness of laminates with fully dense layers largely depends on the work done while ductile ligaments between the crack surfaces are stretched as the crack opens. A key issue in this context is the effect of the constraint imposed by the surrounding ceramic layers, which leads to the effective yield stress being raised appreciably. When the dense metal layers are replaced by metal foams, constraint on plastic deformation will be relieved by the presence of pores, since there can be no stress normal to a free surface. A further difference will arise from changes in the stress field at the crack tip. It is expected that the stress experienced by the succeeding ceramic layer will be lower than would be the case for a fully-dense metal.

It has been demonstrated that, when small scale yielding conditions are applicable, the toughening due to ductile bridging, ΔG_b, is given by[8]

$$\Delta G_b = f_m \sigma_Y \left(\frac{h_m}{2} \right) w \qquad (1)$$

where f_m is the volume fraction of metal, σ_Y the uniaxial yield strength, $h_m/2$ the half-thickness of the (planar) metal ligament and w the "work of fracture" parameter. The magnitude of w can be directly evaluated from the relationship between the stress carried by the constrained layer and the total opening of the crack faces[9].

In the present study, an attempt is made at characterising the deformation of metal foam / ceramic laminates in bending. The systems selected for investigation were Al_2O_3 diffusion-bonded to Al-7Si foam or to Al-12Si-0.6Mg foam. The experimentally measured fracture energy is compared with values predicted using Eqn 1, with work of fracture values obtained from constrained ligament tensile tests.

EXPERIMENTAL PROCEDURE

Materials

Two aluminium foams were employed. The first (F1) was produced by a three-stage melt processing route[10]. These stages were: (1) melting of an Al-7wt%Si ingot, (2) addition to the melt and dispersion of a powder mixture comprising Al-12wt%Si and preoxidized TiH_2 and (3) controlled reaction of the TiH_2 with the melt during solidification. The second foam (F2) was made from an Al-12Si-0.6Mg alloy via a powder-based route[11]. Al alloy powder was mixed with TiH_2 powder, consolidated by extrusion and heated into the semisolid regime.

Materials Characterisation

Both foams exhibit a predominantly closed cell structure (Fig. 1). Images with about 200 cells were produced by optical microscopy of polished sections and analysed using SeeScan software. The cell size was calculated by finding the "diameter" of the pore from the shortest distance between a pair of parallel lines surrounding the pore, so that no part of the pore crossed either line. The cell size was the mean of 36 "diameters", at 5 intervals. The cell size distributions and average cell sizes are given in Fig. 2. It can be seen that foam F1 exhibited both a slightly greater average cell size and a greater spread of sizes than F2. The porosity levels of foams F1 and F2 were measured to be 40% and 73% respectively.

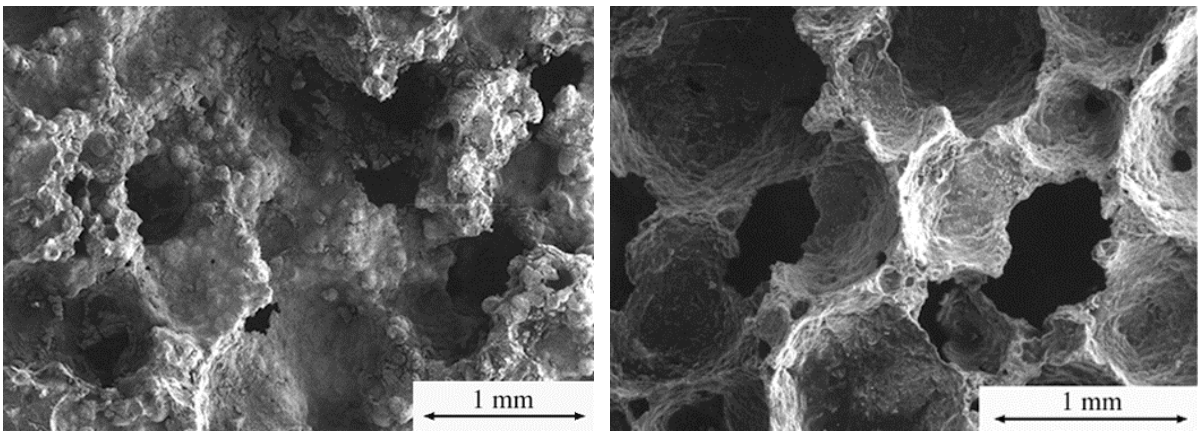

Fig. 1: SEM micrographs of fracture surfaces, showing foam cell structures: (a) foam F1 (Al-7Si) and (b) foam F2 (Al-12Si-0.6Mg). In F1, the dendritic structure formed during melt solidification can be seen, whereas in F2 the material never became fully liquid during processing.

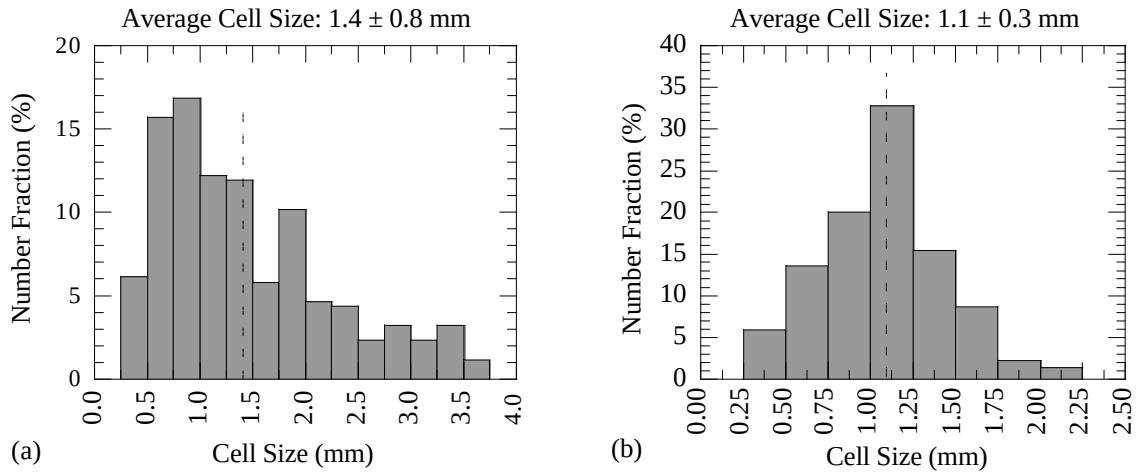

Fig. 2: Cell size distributions for (a) F1 and (b) F2.

Fabrication of Composite Laminates

Two types of specimen were used in the present study: (i) foam/Al_2O_3 sandwich tensile specimens (Fig. 3) and (ii) foam/Al_2O_3 multi-layer laminates. The former were used to examine the *constrained* tensile deformation of the foam layers and the latter to study flexural loading. Laminates consisting of seven alternate layers of Al_2O_3 and F1 or F2 were prepared.

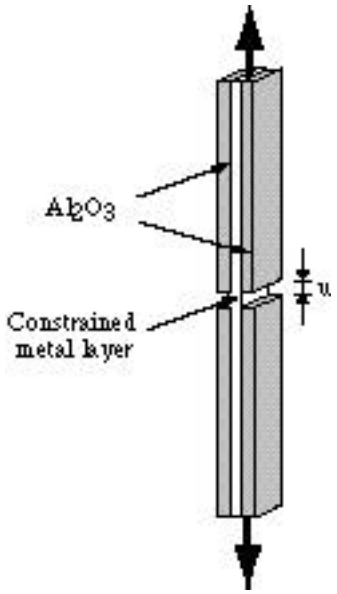

Fig. 3: Schematic of a test specimen designed to measure the work of fracture

The composites were fabricated by diffusion bonding in a large vacuum hot press. The vacuum in the chamber was maintained at 10^{-5} mbar, under a uniaxial pressure of 0.1 MPa. The bonding temperatures were 550 and 560 C, for the Al-7Si and Al-12Si-0.6Mg composites respectively, with a holding time of 4-5 hours. Aluminium spacers were used to prevent the foam from collapsing when heated.

Mechanical Testing

Loading was carried out on a servo-hydraulic machine with a 10 kN load cell. Fracture surfaces were examined by SEM. Foam and fully dense sandwich specimens were loaded in tension at a displacement rate of 0.2 mm min^{-1}. An Instron extensometer with a gauge length of 11.5 mm was used to measure the crack-opening displacement, *u*. Prior to tensile testing,

two symmetrical pre-cracks were introduced into the outer Al_2O_3 layers. In order to ensure that the alumina layers impose an appropriate degree of constraint on deformation of the metallic layer, the initial value of u should be very small. This was achieved by placing a row of Vickers indents along the central plane normal to the specimen axis. Loading in three-point flexure, with the indentations along the line of maximum tension, caused the formation of a sharp crack beyond the ends of the indentations. The crack extended to the Al alloy/Al_2O_3 interface. The width of the crack, u_o, was measured, using an optical interferometric profilometer (WYKO RST Plus), to be about 20-25 μm. Fig. 4 shows a topographic map of the indented and cracked surface.

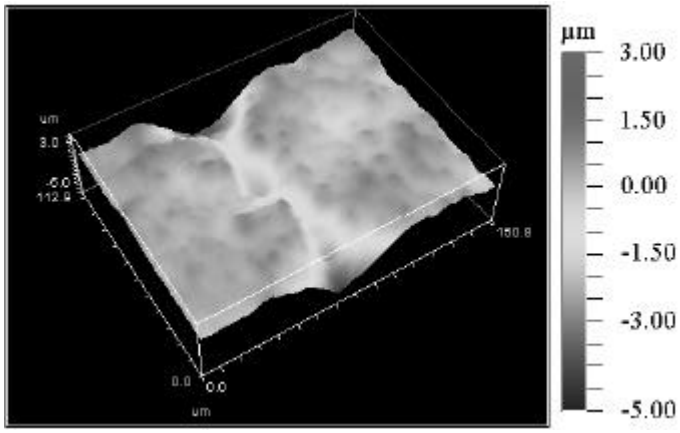

Fig. 4: Optical interferometric topography map, showing the surface of the Al_2O_3 after cracking along a line of indents.

Load-deflection curves were obtained in three-point flexure on laminates with a 25 mm span, using a roller displacement rate of 0.02 mm min^{-1}. Al_2O_3 layers were arranged as the outside layers. Two foam volume fractions, f_f (= h_f / (h_f+h_c), where h is the layer thickness and the subscripts f and c refer to the foam and ceramic respectively), were used, while the Al_2O_3 layers were of constant thickness (1 mm). One face of the specimens was polished, to facilitate observation during and after testing.

RESULTS AND DISCUSSION

Strength of Unconstrained Al-7Si and Al-12Si-0.6Mg foams

The stress-strain curves for F1 and F2 are shown in Fig. 5(a). Plots are shown in Fig. 5(b) for corresponding fully dense alloys in as-cast form. In the initial linear regime of the foams, up to 0.4 and 0.2% for F1 and F2 respectively, cell wall bending and stretching occur[12]. Yielding takes place via plastic bending of cell walls in some regions. Measured yield strengths for F1 and F2 are about 22 MPa and 9 MPa, respectively. Both foams deformed with little or no macroscopic strain hardening. The higher strength of foam F1 is largely attributable to its lower porosity content (40%, versus 73% for F2), although it may also be partly due to the matrix being slightly stronger (see Fig. 5(b)) and the oxide content being lower.

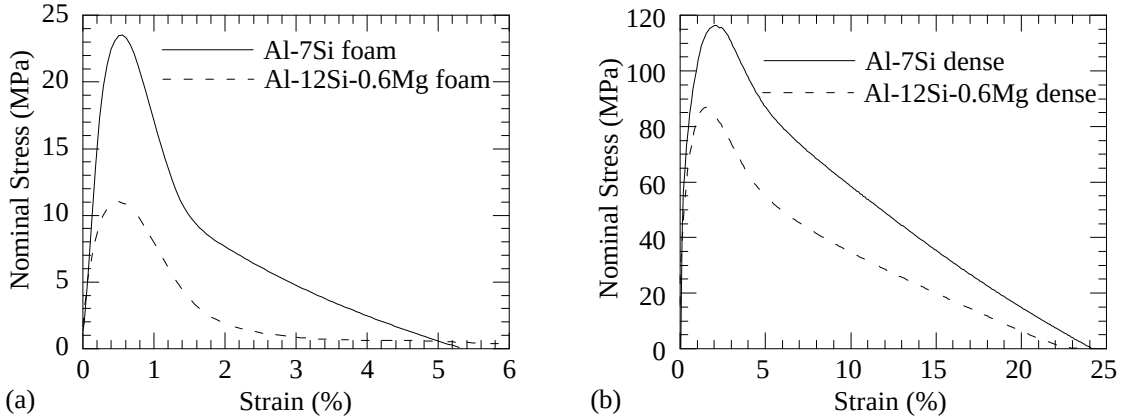

Fig. 5. Stress-strain curves for unconstrained tensile loading of (a) F1(Al-7Si) and F2 (Al-12Si-0.6Mg) and (b) corresponding fully dense alloys in as-cast form.

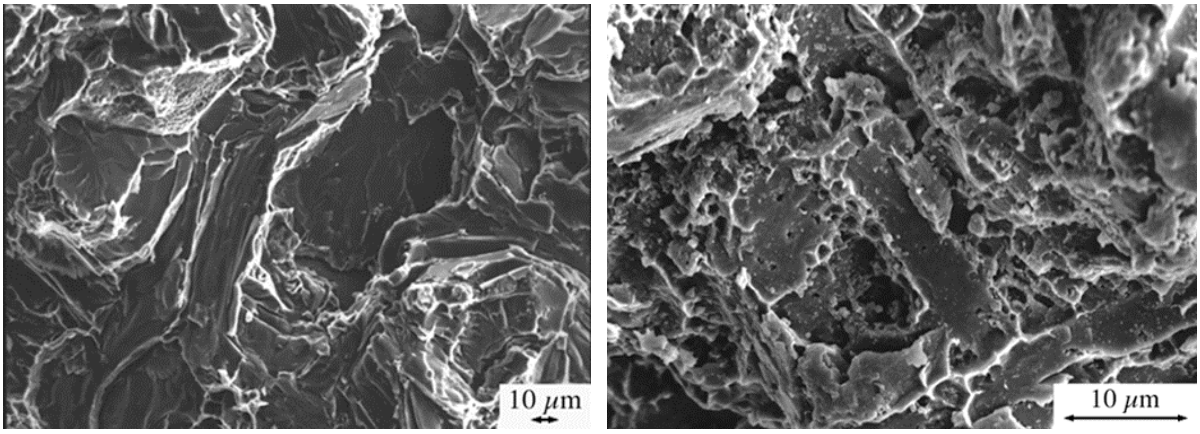

Fig. 6: SEM micrographs of fractured cell walls, showing (a) F1 and (b) F2 foams. Mixed cleavage and ductile features are evident in both.

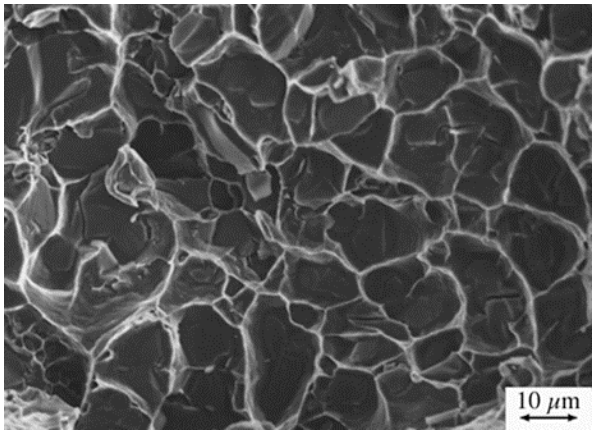

Fig. 7: Fracture surface of dense Al-7Si in the as-cast state.

Once a cell wall had failed (plastically buckled), stress redistribution occurred, causing the stress to reach the plastic buckling stress for other cell walls. This cycle repeated itself until final failure. In most of the specimens, final failure initiated at two sites and generated more than one crack, but only one of them propagated to cause final rupture. Post-fracture observations (Fig. 6) revealed that, in both foams, cell walls failed by a mixture of ductile tearing and brittle fracture. There was no extensive necking of the cell walls in the vicinity of the crack, indicating that the overall plastic deformation was relatively small. In contrast, fracture surfaces of the fully dense alloys (Fig. 7) showed extensive local plasticity. The 0.2%

offset yield stress was about 71 MPa and 56 MPa for fully dense Al-7Si and Al-12Si respectively.

Tensile Tests on Pre-Cracked Sandwich Specimens

Stress-displacement curves are shown in Fig. 8. The axes are the dimensionless variables σ_n/σ_Y and $2u/h$, where σ_n is the nominal stress carried by the constrained layer, σ_Y the uniaxial yield strength, u the crack opening displacement and $h/2$ the semi-thickness of the constrained layer. (The subscripts f and m refer to the foamed and dense metal layer, respectively.)

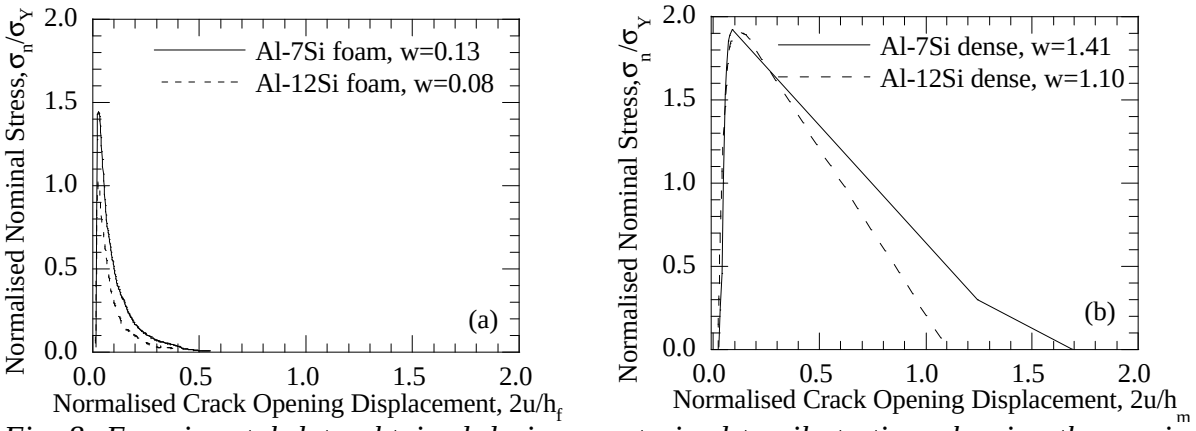

Fig. 8: Experimental data obtained during constrained tensile testing, showing the nominal stress as a function of crack opening displacement for (a) foams and (b) fully dense alloys.

In dense and foamed Al-7Si layers, the plots show a steeply linear rising part up to a maximum, σ_n/σ_Y, of about 1.9 and 1.5 at crack openings, u, of about 63 and 12 μm, respectively. The higher flow stress of the constrained layers compared with the unconstrained values can be attributed entirely to the constraint effect, since no work hardening occurred. The peak stress ratio is lower for the foam layers, since the free surfaces (pores) allow relaxation of the constraint. Additionally, for the fully dense layers, the steeply rising part of the stress-diplacement curve is followed by an approximately linear fall to a normalised opening of about 1.7. In the foam the stress ratio falls more sharply, to a normalised opening of about 0.5, giving a similar shape to that in the unconstrained state. The "work of fracture", w, measured as the area under the normalised curve was equal to 1.41 and 0.13 for fully dense and foam layers, respectively. The difference is attributed both to the higher peak stress ratio and to the higher displacement at failure of the fully dense layer. Similar behaviour was observed for the Al-12Si-0.6Mg layers.

Laminate Flexure Tests

Load-displacement plots from three-point bending experiments on laminates, with foam layer thickness, h_f, of 2 and 3 mm, are shown in Fig. 9. For both of the curves in Fig. 9(a), the initial response is approximately linear, possibly showing a small deviation from linearity before the first load drop. Further increase in load is non-linear and is marked by a distinct load drop. Direct in situ observations of specimens at this point revealed that cracks had been formed in all the ceramic layers. Further deformation led to a progressive load decrease, corresponding to plastic deformation of the foam layers. The F2 laminates (Fig. 9(b)) showed similar features.

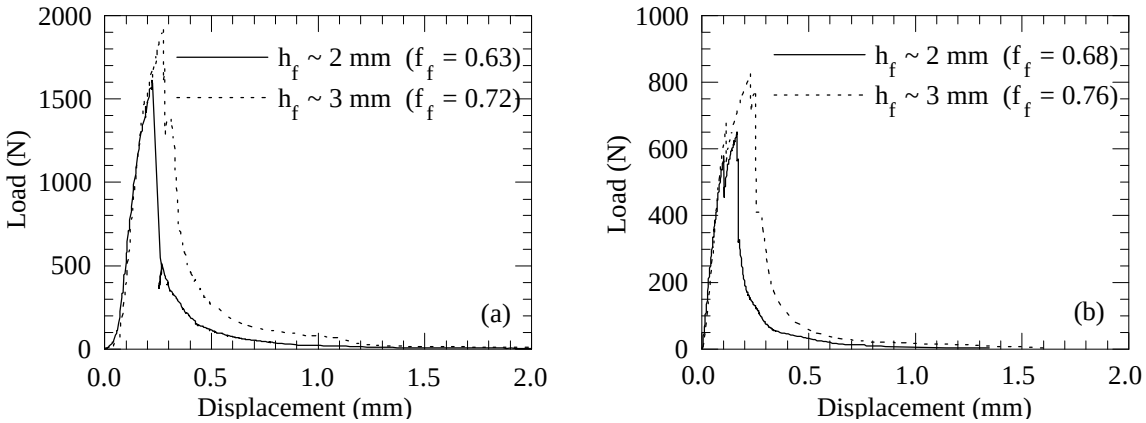

Fig. 9: Flexural load-displacement plots for (a) F1/Al_2O_3 and (b) F2/Al_2O_3 laminates

Fig. 10 shows the side surface of an Al-12Si-0.6Mg laminate and reveals that failure occurred with a step-like displacement. The resulting crack path displays a series of steps of different width at each layer. Crack deflection is thought to arise from the presence of weakened interfaces, due to the reduced contact area associated with a foam. The debond length was generally of the order of 1 mm. As the debond crack encounters a fracture-resistant region, the crack is arrested and kinks into the next layer, rather than continue along the interface. In the foam layer, the crack follows the trajectory with the lowest resistance. Regions with high porosity, and therefore cells with thin cell walls, are preferred routes for crack growth.

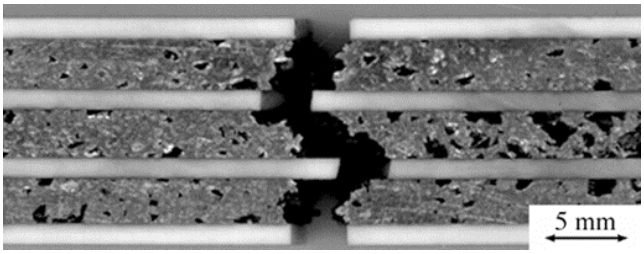

Fig. 10: Crack path in an F2/Al_2O_3 laminate

Estimation of the fracture energy involves obtaining the area under the load-displacement curves and then dividing by the fracture cross section. Comparison of the load-deflection curves (Fig. 9) for the two laminates with h_f values of 2 and 3 mm reveals that the area under the curve as well as the peak load increase with increasing thickness of the foam layer. (The Al_2O_3 layers have constant thickness). Moreover, the load drop seems to stop at a level dependent on the thickness of the foam layer, e.g. the load drop stops at a higher load as the foam layer thickness rises.

When small scale bridging conditions are applicable, the incremental toughening of the composite, for a ductile ligament, can be related to the work of stretching and fracture of the bridging ligament[8] (see Eqn 1). Thus the fracture energy of the composite, G_{tot}, can be calculated from the constrained single foam layer model using the following expression

$$G_{tot} = G_{cer}(1 - f_f) + f_f \sigma_Y \left(\frac{h_f}{2} \right) w \qquad (2)$$

where G_{cer} is the fracture energy of the ceramic.

Expressing the second term on the right hand side of Eqn 2 in terms of the foam volume fraction, f_f, it becomes

$$G_{\text{tot}} = G_{\text{cer}}(1-f_{\text{f}}) + \frac{w}{2} h_{\text{c}} \sigma_{\text{Y}} \left(\frac{f_{\text{f}}^2}{1-f_{\text{f}}} \right) \tag{3}$$

The fracture energy of polycrystalline Al_2O_3, G_{cer}, has been estimated[13] at between 10 and 100 J m^{-2}, depending on the crack length. In the current study, a constant value of 25 J m^{-2} has been taken[14]. Moreover, from the tests on constrained fracture of F1 and F2 foams, the work of fracture, *w*, was found to be 0.13 and 0.08 respectively. The value of h_C was constant in all the experiments at 1 mm. Concerning σ_Y, based on the stress-strain curve in Fig. 5, it can be seen that the flow stresses do not change much with strain, i.e. there is little work hardening. Therefore, for the purpose of energy predictions, the flow stresses were taken as constant ($\sigma_{Y(F1)}$ = 22 MPa, $\sigma_{Y(F2)}$ = 9 MPa). The fracture energies of the two foams are thus given by these two expressions

$$G_{\text{tot(F1)}} = 25(1-f_{\text{f}}) + 1430 \left(\frac{f_{\text{f}}^2}{1-f_{\text{f}}} \right) \tag{4}$$

$$G_{\text{tot(F2)}} = 25(1-f_{\text{f}}) + 360 \left(\frac{f_{\text{f}}^2}{1-f_{\text{f}}} \right) \tag{5}$$

Likewise, using the values of *w* for the dense F1 and F2 layers (1.41 and 1.10 respectively), the predicted fracture energies of the dense metal layer laminates are plotted in Fig. 11 against the metal volume fraction. Also, results from laminate flexure are shown in the graph.

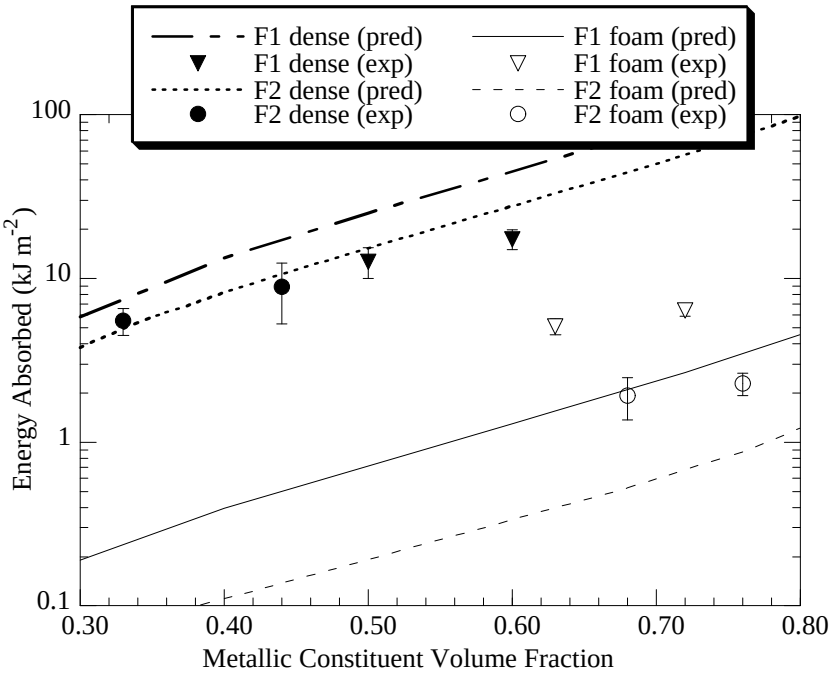

Fig. 11: Comparison between predicted and experimentally measured fracture energy of F1 and F2 foam / Al_2O_3 laminates. The theoretical plots correspond to predictions using Eqns 4 and 5. Experimental data were obtained from laminate flexure. Predictions and experimental data for the corresponding fully dense laminates are also shown.

In Fig. 11, predicted fracture energies are compared with experimental data. While the effects of foam content and strength (yield stress) are correctly predicted, the experimental values are greater than the theoretical ones by a factor of about 3. This may be partly attributable to the contribution from interfacial debonding, although, since the interfacial fracture energy has been

measured to be only a few $J\,m^{-2}$, the contribution from this source is probably not very significant. However, interfacial debonding may have led to significant work being done by frictional sliding as the crack opens up, particularly in view of the fact that the measurements were made in bending, which can accentuate the interference between the crack flanks as they disengage. For the corresponding dense metal laminates, on the other hand, the experimental fracture energies are slightly lower than the predicted values. In view of the greater toughnesses, any contribution from frictional sliding is expected to be much less significant in these cases.

CONCLUSIONS

A study has been made of the failure mechanisms in foam-containing laminates under flexural and tensile loading. The main conclusions are outlined below.

1. Tensile testing of single metallic foam layers (and corresponding fully dense metals) sandwiched between pre-cracked ceramic layers has been employed in order to study their deformation characteristics when constrained in this way. Both dense and foamed layers show initial linear rises in load with increasing strain, followed by a drop to zero load as necking and rupture occurs. The loads, expressed as a nominal stress and normalised by the yield stress of corresponding unconstrained material, show lower peaks for the foams than for the dense metals. The strains to failure are also reduced. These effects are attributed respectively to the reductions in constraint and in ductility when pores are present.

2. Fracture energies were measured in laminate bending. It was found that the absorbed energy increased as the proportion of foam in the laminate increased. Flexural failure occurred by propagation of a single non-planar crack. The resulting crack front displayed a series of steps at each layer.

3. Comparison between the fracture energies obtained experimentally from laminate flexure and the predicted values, obtained using a previously-developed model based on the work of stretching the bridging ligaments, showed good agreement in terms of the effects of foam content and foam strength. The absolute values, which are considerably lower than for corresponding dense metallic layers, are also correctly predicted in terms of their order of magnitude. However, the experimental values are significantly higher than the predicted ones. It is suggested that the difference may arise from frictional sliding between crack flanks as they disengage, which assumes a greater importance relative to the case of fully dense metal layers in view of the lower contributions from ligament deformation.

ACKNOWLEDGEMENTS

One of the authors (AEM) gratefully acknowledges the provision of funding from the State Scholarships Foundation (SSF) of Greece.

REFERENCES

1. Pateras, S.K., Shaw, M.C., Clegg, W.J., Cocks, A.C.F. and Clyne, T.W., "The Effect of Metal Layer Thickness on Energy Absorption during Fracture of Metal/Ceramic Laminates", *Proceedings of the Tenth International Conference on Composite Materials (ICCM10)*, Whistler, British Columbia, Canada, August 14-18, 1995, Vol. I: Fatigue and Fracture, Poursartip, A. and Street, K., Eds, pp. 731-737.

2. Cao, H.C. and Evans, A.G., "On Crack Extension in Ductile/Brittle Laminates", *Acta Metall. Mater.*, Vol. 39, No. 12, 1991, pp. 2997-3005.

3. Chen, Z. and Mecholsky, J.J., "Toughening by Metallic Lamina in Nickel/Alumina Composites", *J. Am. Ceram. Soc.*, Vol. 76, No. 5, 1993, pp. 1258-1264.

4. Pateras, S.K., Howard, S.J. and Clyne, T.W., "The Contribution of Bridging Ligament Rupture to Energy Absorption during Fracture of Metal-Ceramic Laminates", *Key Eng. Mats.*, Vol. 127-131, No. , 1997, pp. 1127-1136.

5. Shaw, M.C., Clyne, T.W., Cocks, A.C.F., Fleck, N.A. and Pateras, S.K., "Cracking Patterns in Ceramic/Metal Laminates", *J. Mech. Phys. Solids.*, Vol. 44, No. 5, 1996, pp. 801-814.

6. Howard, S.J., Pateras, S.K. and Clyne, T.W., "The Effects of Interfacial Debonding and Work Hardening on the Fracture of Metal-Ceramic Laminates", *Proceedings of the Eleventh International Conference on Composite Materials (ICCM-11)*, Gold Coast, Queensland, Australia, July 14-18, 1997, Vol. III: Metal Matrix Composites, Scott, M. L., Ed, pp. 260-273.

7. Howard, S.J., Pateras, S.K. and Clyne, T.W., "The Effect of Interfacial Adhesion on the Toughness of Metal/Ceramic Laminates", *Mat. Sci. & Tech.*, Vol. 14, No. 6, 1998, pp. 535-541.

8. Evans, A.G. and McMeeking, R.M., "On The Toughening of Ceramics by Strong Reinforcements", *Acta Metall.*, Vol. 34, No. 12, 1986, pp. 2435-2441.

9. Mataga, P.A., "Deformation of Crack-Bridging Ductile Reinforcements in Toughened Brittle Materials", *Acta Metall.*, Vol. 37, No. 12, 1989, pp. 3349-3359.

10. Gergely, V. and Clyne, T.W., "The Effect of Oxide Layers on Gas-generating Hydride Particles during Production of Aluminium Foams", *Porous and Cellular Materials for Structural Applications*, Part III: Manufacture of Solid Foams, Schwartz, D. S., Shih, D. S., Evans, A. G. and Wadley, H. N. G., Eds, Materials Research Society, San Francisco, 1998, pp. 139-144.

11. Simancik, F., Degischer, H.P. and Wörz, H., "Foamed Aluminium-Light Structural and Insulation Material", *Proceedings of the Fourth European Conference on Advanced Materials & Processes (Euromat '95)*, Venice/Padua, Italy, September 28, 1995, Vol. IV: Structural Metallic Materials, pp. 191-196.

12. Gibson, L.J. and Ashby, M.F., *Cellular Solids*, 2nd Edition, Cambridge University Press, Cambridge, 1997.

13. Vekinis, G., Ashby, M.F. and Beaumont, P.W.R., "R-Curve Behaviour of Al_2O_3 Ceramics", *Acta Metall. Mater.*, Vol. 38, No. 6, 1990, pp. 1151-1162.

14. Flinn, B.D., Zok, F.W., Lange, F.F. and Evans, A.G., "Processing and Properties of Al_2O_3-Al Composites", *Mater. Sci. Eng.*, Vol. A144, 1991, pp. 153-157.